

Corrosion Resistance of as-rolled Mg-Li-AlSi Alloys

Zilong Zhao^{1,2}, Yiding Liu^{1,2}, Yifeng Zhong^{1,2*}, Xianhua Chen³, Zhiqiang Zhang⁴

¹ School of Civil Engineering, Chongqing University, Chongqing 400045, China

² Key Laboratory of New Technology for Construction of Cities in Mountain Area (Chongqing University), Ministry of Education, Chongqing 400045, China

³ College of Materials Science and Engineering, Chongqing University, Chongqing 400045, China

⁴ Key Lab of Electromagnetic Processing of Materials, Ministry of Education, Northeastern University, 314Mailbox, Shenyang 110819, China

*E-mail: 529972463@qq.com

Received: 11 December 2017 / Accepted: 5 March 2018 / Published: 10 April 2018

In this paper, single α -phase alloys (Mg-4Li, Mg-4Li-3AlSi) and single β -phase alloys (Mg-12Li, Mg-12Li-3AlSi) were used as the research object. The corrosion behaviors of four alloys in 3.5wt% NaCl solution are investigated. The influence of elemental Al and Si on the corrosion resistance of the alloy is revealed. The corrosion resistances of α -phase alloy Mg-4Li and Mg-4Li-3AlSi are obviously better than that of β -phase alloy Mg-12Li and Mg-12Li-3AlSi. The addition of Al-Si master alloy could increase the rate of hydrogen evolution and decrease the corrosion resistance of the alloy. The surface phase of the Mg-Li-AlSi is mainly consist of α -Mg, β -Li, Mg(OH)₂, Al₂O₃ and Mg₂Si.

Keywords: Al-Si eutectic, Mg-Li alloys, precipitation, corrosion, rolling

1. INTRODUCTION

Magnesium and its alloys are among the lightest of all structural metals, significantly lighter than steel, titanium and aluminum alloys [1, 2]. Therefore, it has become one of the potential engineer materials for automobile and aeronautical industries because of its high strength weight ratio and low density [3-5]. In order to obtain excellent properties and wide applications, many researchers have paid great attention to explore effective strengthening phases in Mg alloys [6-9]. Although Mg alloys possess good strength-to-weight ratios and performance, there are two key factors preventing them from being used as possible structural materials. One factor is that cold workability (near room temperature) is limited. Because it is very difficult to overcome owing to the hexagonal closed-packed (HCP) crystal structure of Mg (which possesses few slip systems during deformation). Another factor is high susceptibility to be corroded. This point is particularly critical for Mg alloys reported so far as

they do not form a protective oxide film on their surface (as opposed, for example, to aluminum, stainless steel or titanium alloys). Moreover, Mg alloys have no effective sacrificial coatings similar to those of zinc on steel surfaces [1, 10].

Obviously, it is important to improve their ability to withstand corrosion. Up to now, various approaches, including anodizing, conversion coating, electroplating, and vapor deposition, have been proposed to improve the corrosion resistance of magnesia based alloys [11-12]. Wu et al. reported the corrosion resistance of magnesium-aluminum alloy and preparing surface coating by hydrothermal method [13-18]. Liu et al. reported that hot corrosion behavior of two-step Mg-Al spinels in molten electrolyte. [19-22].

Because of high specific strength, high specific stiffness, excellent damping capabilities, and good electromagnetic shielding properties, Mg-Li alloys possess the potential for using in areas such as spaceflight, weapons and automobile manufacturing. For this reason, recently, Mg-Li alloys have attracted extensive interests of researchers and are becoming a hot topic [23-26]. The Mg-Li binary alloy phase diagram [27] shows that the alloy maintains its HCP-structured single-phase (solid solution of lithium in magnesium, α -Mg) when Li content is below 5.5wt%, exhibits a duplex structure containing both HCP-structured α -Mg and BCC-structured β -Li (solid solution of magnesium in lithium, α + β -Mg) when Li content is between 5.5wt% and 11wt%, and transforms into a BCC-structured single-phase (β -Mg) when Li content exceeds 11wt% [28]. Zhao reported the corrosion resistance of Mg-8Li alloy [29], but the comparison of corrosion resistance for single α -phase and single β -phase in Mg-Li alloy and their corrosion mechanism were not reported. The role of Al and Si elements in the corrosion process is seldom mentioned. In this paper, a single α -phase alloy (Mg-4Li, Mg-4Li-3AlSi) and a single β -phase alloy (Mg-12Li, Mg-12Li-3AlSi) were used as the research object, the corrosion behavior and mechanism of different phase alloy in 3.5wt% NaCl solution are studied. At the same time, the influence of adding Al and Si on the corrosion resistance of the alloy is also studied.

2. EXPERIMENTAL

2.1. Materials and sample preparation

The magnetic levitation vacuum high frequency induction melting technique is applied in this experiment. The pure magnesium, pure lithium and Al-Si eutectic alloy with 12.6wt% Si (all in mass, unless otherwise stated) were melted under argon atmosphere and rapidly cooled down by water in the copper mold with dimensions of Φ 30 mm \times 60 mm. Four alloys Mg-4Li, Mg-4Li-3(Al-Si), Mg-12Li and Mg-12Li-3(Al-Si) were prepared, where the numbers mean the nominal weight percentage contents of Li element or Al-Si eutectic in the alloys. After casting, the ingots were cut into round plates of Φ 30 mm \times 10 mm, and annealed at 300 °C for 1 h. The plates were rolled into the sheets of 1.6 mm thick after multi-pass rolling with a thickness reduction of about 20% for each pass. The rollers with a diameter of Φ 130 mm were preheated to 150 °C and held at which throughout the rolling procedure. Finally, the rolled specimens were annealed at 150 °C for 60 min.

2.2. Corrosion and electrochemical tests

Four kinds of rolled-annealed alloy samples (10×15 mm) in 3.5 wt% NaCl solution were used in hydrogen evolution corrosion test. Free immersion with no external polarization in 3.5wt%NaCl solution was carried out and samples of anodic polarization were tested in 3.5wt%NaCl solution. All the test solutions were prepared by laboratory - level reagents and deionized water. The solution is not degassed. Using a solution of 350mL in each test. The morphologies of the surfaces were observed by using an optical microscope (OM, LEICA DM 2500M). The microstructure and composition were examined by using a MIRA3 scanning electron microscope (SEM, Nova 400 FEI, USA) equipped with an Oxford X-ray energy dispersive spectroscope (EDS INCA Energy 350 Oxford, UK). An X-ray diffractometer (XRD, D/Max 2500X Rigaku, Japan) was employed to examine the crystal structure of the alloys.

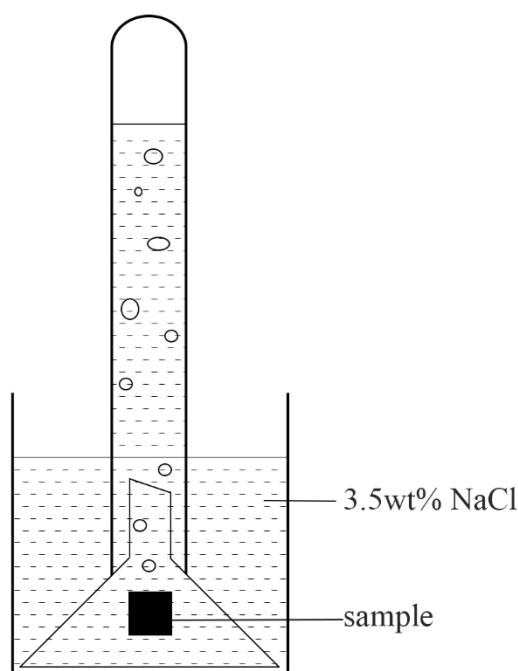


Figure 1. Corrosion test of four kinds of rolled-annealed alloy samples in 3.5 wt% NaCl solution

Potentiodynamic polarization curves and EIS were obtained at room temperature in a cell with 3.5 wt% NaCl solution using CIMPS-2 Zahner. A classical three-electrode system was used with the sample as the working electrode (1cm²), an SCE as the reference electrode, and a platinum plate as the counter electrode. Polarization curves for all samples were obtained by automatically changing the electrode potential from -2 V in the cathodic direction to 0.5 V in the anodic direction with reference to the open circuit potential (OCP) at a sweep rate of 2 mV s⁻¹. Impedance measurements were swept by a 10 mV rms sinusoidal perturbation and performed at OCP from 10 mHz to 100 kHz, with 10 experimental points collected per frequency decade above 66 Hz and 5 experimental points collected per frequency decade below 66 Hz. The experimental impedance plots were fitted using different

equivalent circuits by means of the Zview software. All polarization and EIS tests were carried out at room temperature. In order to ensure the reproducibility, there were three parallel samples in each system.

3. RESULTS AND DISCUSSION

Fig.2 shows OM images of various as-rolled Mg-4Li and Mg-12Li alloys. After corroded by 3% nitric acid alcohol corrosion solution, the four alloys showing different structures and corrosion resistance. The corrosion results are consistent with the hydrogen evolution effect in NaCl solution. It can be seen from the figure that the Mg-4Li alloy is equiaxed structure in rolled and annealed state and others are banded microstructure, which is consistent with the result in Ref.[3]. Compared with Mg-4Li and Mg-4Li-3AlSi, Mg-12Li and Mg-12Li-3AlSi, it can be seen that after adding Al-Si master alloy, there are more corrosion points on the surface of Mg-4Li-3AlSi and Mg-12Li-3AlSi alloy, the corrosion resistance of the alloy is obviously worse. In addition, compared with the OM images of Mg-4Li and Mg-12Li, it can be seen that the OM images of Mg-12Li is a band-like microstructure and the grain size of the flattened grains is very large, the corrosion points of surface are obviously more than those of Mg-4Li, indicating that the corrosion resistance of Mg-4Li is better than that of Mg-12Li, which is consistent with the results of hydrogen evolution.

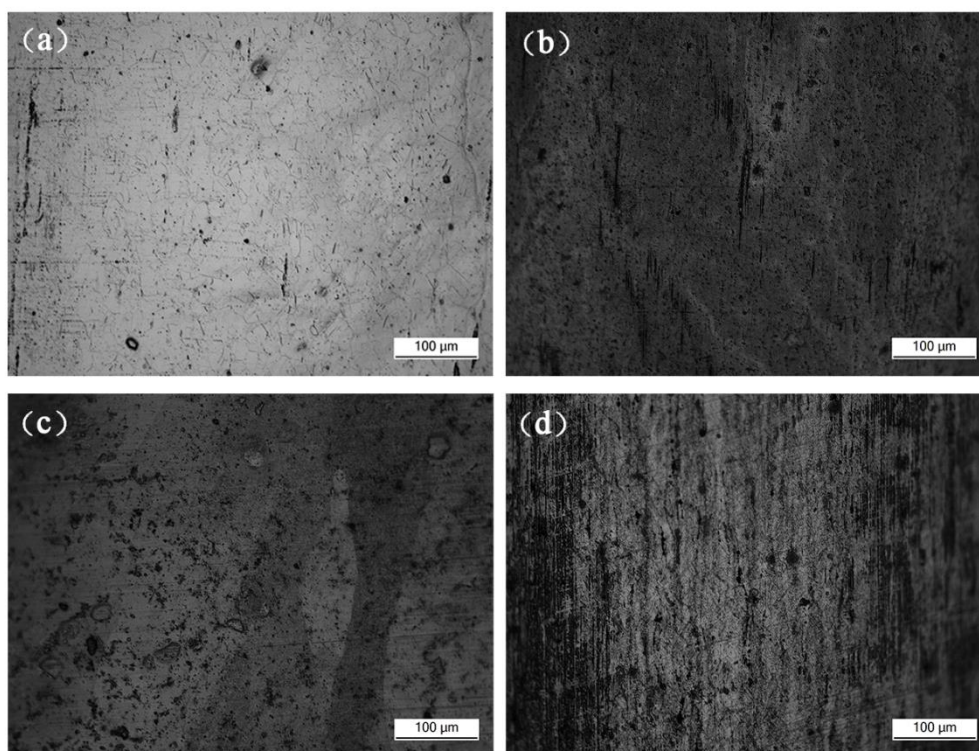


Figure 2. OM image of various as-rolled Mg-4Li and Mg-12Li alloys: (a) Mg-4Li, (b) Mg-4Li-3AlSi, (c) Mg-12Li, (d) Mg-12Li-3AlSi.

Fig.3 shows the SEM images of Mg-4Li and Mg-12Li alloys after hydrogen evolution. In Fig.3a, it can be seen that the hydrogen evolution area of Mg-4Li alloy surface is non-uniform. The gray area formed by fierce hydrogen evolution reaction, and the black area formed by weak hydrogen evolution reaction. The grey area almost covers the Mg-4Li-3AlSi surface, because of the addition of Al-Si master alloy, the second phase Mg₂Si and Al₃Li even distribution [3], which leads to alloy corrosion points increasing and the accelerated rate of hydrogen evolution. This is also the main reason that the hydrogen evolution rate of Mg-4Li-3AlSi is higher than that of Mg-4Li alloy. In comparison with Fig.3a and Fig.3c, all areas on the Mg-12Li surface are grey hydrogen evolution regions and a small amount of cracks existe. This is the main reason that the hydrogen evolution rate of Mg-12Li is higher than that of Mg-4Li and Mg-4Li-3AlSi alloy. It is further explained that the corrosion resistance of Mg-4Li (α -phase) in NaCl solution is better than that of Mg-12Li (β -phase). Finally, in comparison with Fig.3c and Fig.3d, it can be seen that the surface of Mg-12Li-3AlSi alloy has a large number of cracks after hydrogen evolution, indicating that the surface hydrogen evolution is intense, so it has the highest hydrogen evolution rate. It is concluded that both the Mg-4Li (α -phase) and the Mg-12Li (β -phase) alloy, the addition of Al-Si master alloy would cause the increase of the hydrogen evolution rate and the decrease of the corrosion resistance.

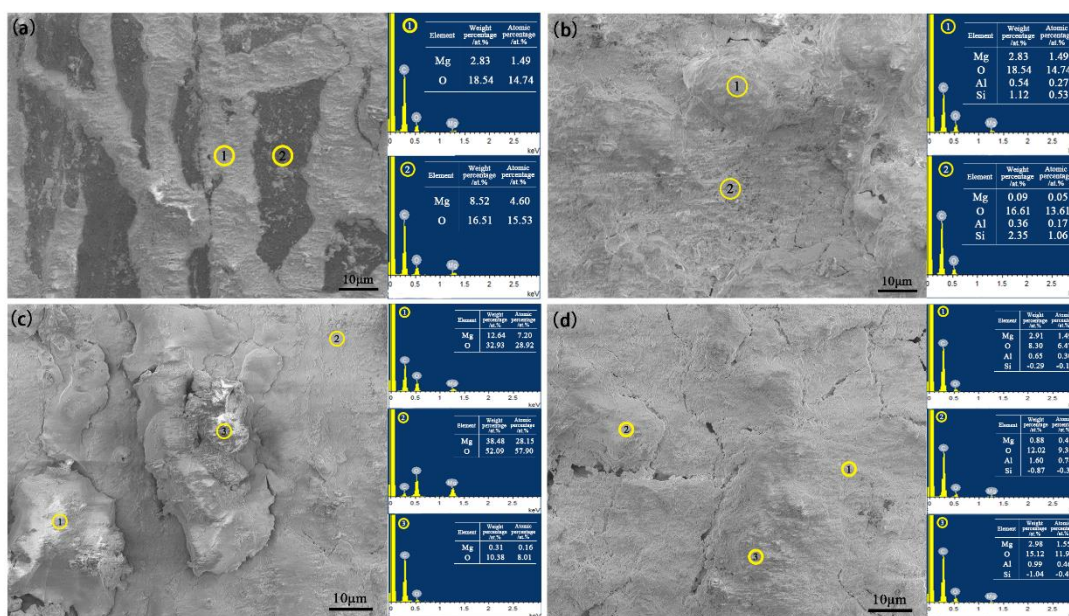


Figure 3. SEM surface images of as-rolled Mg-4Li and Mg-12Li alloys after hydrogen evolution: (a) Mg-4Li, (b) Mg-4Li-3AlSi, (c) Mg-12Li, (d) Mg-12Li-3AlSi. The EDS analysis of ten different positions.

In order to further determine the elemental composition of the alloys surface product after hydrogen evolution, EDS analysis was carried out on the four alloys. Fig.3 (a) are hydrogen evolution SEM image and EDS of as-rolled Mg-4Li alloys. The gray and black areas of Mg-4Li (α -phase) alloy after hydrogen evolution are obviously different. The mass ratio of Mg in the gray region is 2.83%,

which is less than 8.52% of the black area. It shows that hydrogen evolution in gray areas is more intense, which is consistent with the observed result in SEM. Fig. 3(b) are SEM image after the hydrogen evolution and EDS of as-rolled Mg-4Li-3AlSi alloys. It can be seen that the corrosion product after hydrogen evolution tests contains elemental Mg, Al and Si, hydrogen evolution and corrosion effect are different in different regions. The protruding region 1 is dense, and the Al content is 0.54% and the Mg content is 2.83%. In the process of hydrogen evolution, Al reacts with O in water. This reaction forms Al_2O_3 which is a passivation film [30], prevents the reaction from further intensifying. Therefore, the region 1 is compact and has low Si content (1.12%). The structure of the region 2 is loose and porous, there is no Al_2O_3 passivation film formed on the surface, and the content of Si is 2.35%. It shows that Si is the main element that affects the corrosion resistance of Mg-4Li-3AlSi alloy, accelerates the corrosion of the alloy and causes a higher hydrogen evolution rate. Fig.3 (c) shows SEM image after the hydrogen evolution and EDS of product on the as-rolled Mg-12Li alloys surface, as it can be seen from the diagram, the Mg content of region 1,2,3 is 12.64%, 38.48% and 0.31%, respectively. The content of Mg in region 1 and region 2 is higher and the structure is relatively dense, which indicates that there is less corrosion points in Mg-12Li alloy. The corrosion factors are mainly concentrated in region 3. During the hydrogen evolution process, the non-uniform surface area in NaCl solution is preferentially eroded to form a relatively loose hydrogen evolution reaction region. The rate of hydrogen evolution reaction has a great difference in different regions of the surface. Mg could form a insoluble precipitate $\text{Mg}(\text{OH})_2$ in NaCl solution [27]. As time goes on, there were more insoluble precipitate $\text{Mg}(\text{OH})_2$ produced, which hindering the intensification of hydrogen evolution reaction, and obviously reducing the hydrogen evolution rate. Fig.3 (d) shows the hydrogen evolution SEM image and EDS of as-rolled Mg-12Li-3AlSi alloys. It can be seen from the EDS that the surface of Mg-12Li-3AlSi (β -phase) has a large number of cracks. Compared with the 1, 2, and 3 regions, it can be found that the alloy is relatively dense. The content of Al is 0.65%, 1.6% and 0.99%, respectively, indicating that the compact site has Al_2O_3 passivation film protection. The reason why the Si element can't observe in three regions is that Si element is the main corrosion point for accelerating the hydrogen evolution and mainly distributes in the middle of the loose cracks. Therefore, Mg-12Li-3AlSi maintains a high hydrogen evolution rate during the whole hydrogen evolution process. Compared with the dense and relatively uniform Mg-4Li (α -phase) alloy, Mg-12Li and Mg-12Li-3AlSi (β -phase) alloy has many loose points on the surface, the hydrogen evolution rate increases.

Fig. 4 shows the XRD pattern of the four alloys' corrosion products after hydrogen evolution experiment. As it can be seen from the results, Mg-4Li and Mg-4Li-3AlSi are single α -phase structure, while Mg-12Li and Mg-12Li-3AlSi are single β -phase, and there are $\text{Mg}(\text{OH})_2$ phases on the surface of the four alloys. This is consistent with the reaction of hydrogen evolution in Ref.[31]. The peak value of $\text{Mg}(\text{OH})_2$ phase in Mg-12Li alloy increases obviously after hydrogen evolution. The lithium oxide is not observed in XRD results, it is possible that the content of Li in the alloy is low and the generated LiOH is mostly dissolved in the NaCl solution, resulting in XRD devices failing to detect peak of lithium oxide. In addition, Al_2O_3 and Mg_2Si phases are observed in the corrosion products of Mg-4Li-3AlSi and Mg-12Li-3AlSi alloys after hydrogen evolution experiment. In particular, Al_2O_3 phase can gain bigger peak value, which further indicates that the formation of Al_2O_3 passivation film

in the surface products is the main reason for the decrease of hydrogen evolution rate in the late stage. The peak value of Mg_2Si phase in Mg-4Li-3AlSi alloy surface products is relatively strong, which is consistent with the EDS analysis result in Fig.4. The main reason for the weak peak in Mg-12Li-3AlSi is that Si mainly exists in the middle of cracks and almost undetectable on the surface, which is consistent with the EDS analysis results in Fig.3. The surface phases of the alloys after hydrogen evolution are further confirmed to be α -Mg, β -Li, $Mg(OH)_2$, Al_2O_3 and Mg_2Si by XRD analysis.

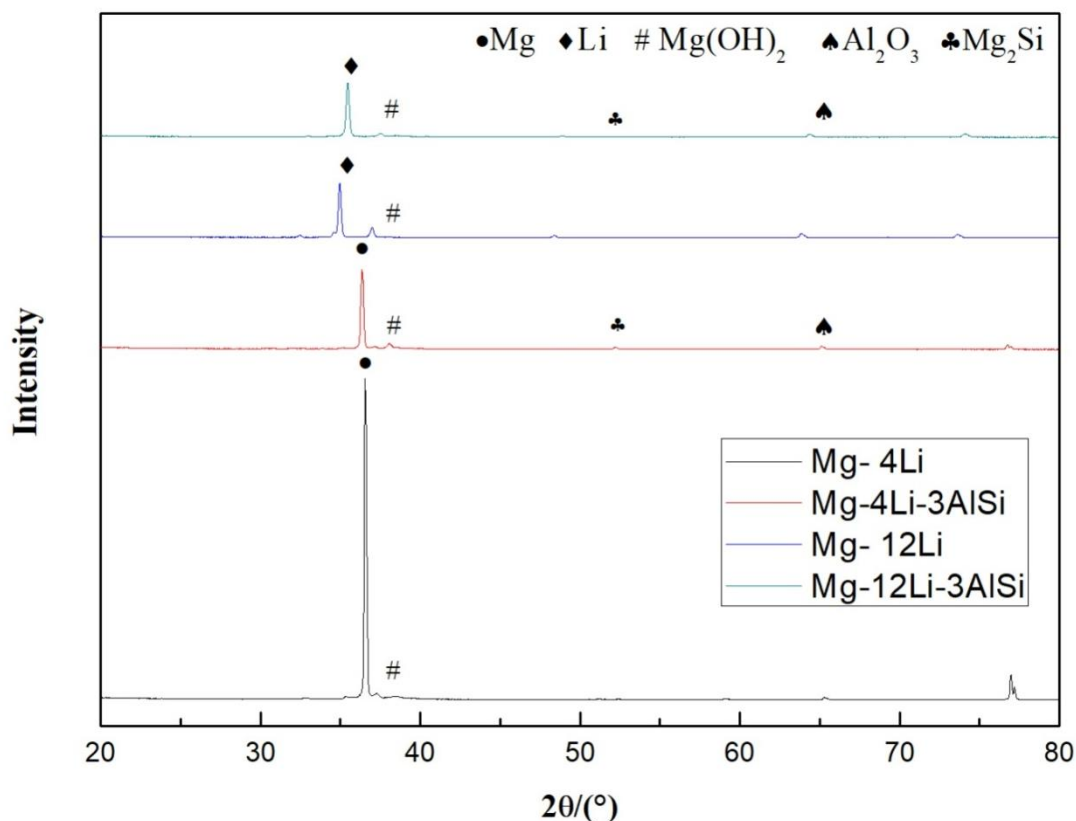


Figure 4. XRD patterns of as-rolled Mg-4Li and Mg-12Li alloys after hydrogen evolution.

Hydrogen evolution curves of Mg-4Li, Mg-4Li-3AlSi, Mg-12Li and Mg-12Li-3AlSi are shown in Fig.5. It can be seen from the figure that the corrosion resistances of α -phase alloys (Mg-4Li and Mg-4Li-3AlSi) are much better than that of β -phase alloys (Mg-12Li and Mg-12Li-3AlSi). The corrosion resistance of the alloys is obviously deterioration after adding elemental Al-Si. During the first 20 minutes of hydrogen evolution, the hydrogen evolution rate of Mg-4Li-3AlSi and Mg-12Li-3AlSi is significantly higher than that of Mg-4Li and Mg-12Li. Due to the addition of Al-Si, the alloys form intermetallic compounds Mg_2Si and Mg_xLi_y phase [3,29], which acts as a weak point to allow hydrogen evolution to proceed at the rate of electrochemical corrosion. With the increase of hydrogen evolution times, the hydrogen evolution rate of the four alloys is also increasing. The hydrogen evolution rate of the β -phase alloy Mg-12Li exceeds that of Mg-4Li-3Al-Si at 30 minutes, which may due to poor β -phase alloys are corroded. After 60 minutes, the hydrogen evolution rate of each alloys is

maintained at a stable higher level, and the corrosion spots of the alloys are completely exposed to NaCl solution during this period. As time goes on, more corrosion products are produced, gradually covering the surface of the alloy to prevent further corrosion. Therefore, after 130 minutes, the hydrogen evolution rate of the four alloys begins to decrease, but still maintain at a high level.

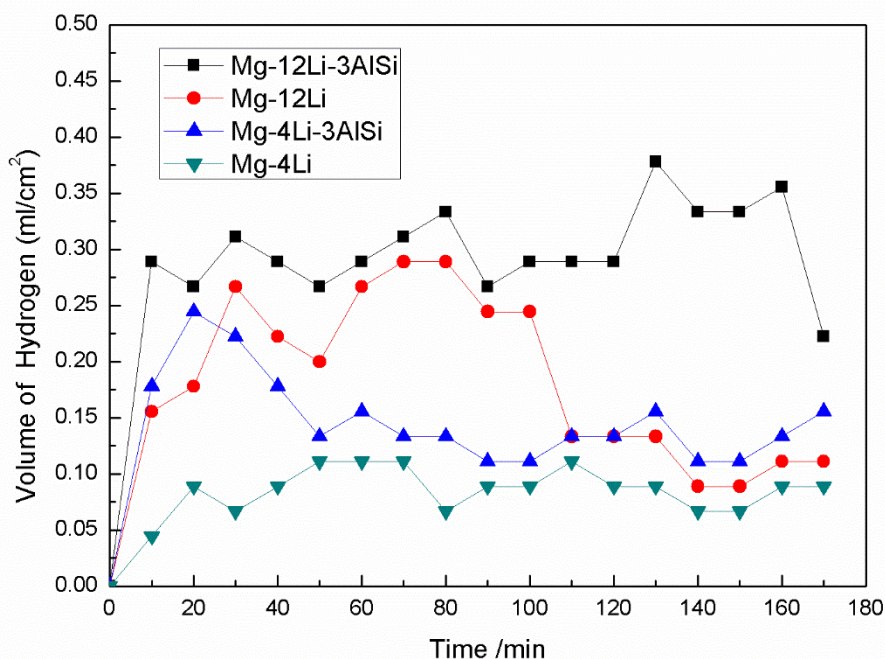


Figure 5. Hydrogen evolution curves of the as-rolled Mg-xLi-(Al-Si) alloys

Fig. 6 shows the potentiodynamic polarization curves of different alloys in 3.5 wt% NaCl solution. It can be seen from the figure that the polarization curves of the four alloys are similar. In the cathode range, hydrogen releases with an increase of potential, resulting in a decrease current densities. In the case of anodic branches, the corrosion current densities increase slowly with increasing anodic potentials. These data further confirm the conclusion. The cathodic branches of all the samples are linear in a large potential range. The corrosion potential of Mg-4Li is the most significant among the four samples, followed by Mg-12Li, both of which are higher than that of Mg-4Li-3AlSi and Mg-12Li-3AlSi. However, different polarization behaviors are showed during the anodic polarization process. Compared with other samples, the current density of Mg-4Li alloy increase rapidly with the increase of electric potential. When the potential is higher than -0.498 V (vs. SCE), the current density of the alloy is the largest. This result shows that Mg-4Li has the highest anodic dissolution activity. The corrosion potential (E_{corr}) and corrosion current density (i_{corr}) obtained by polarization measurements are shown in Table 1. The corrosion current densities of the four specimens are evaluated from the corresponding polarization curves by Tafel extrapolation using the cathode branches [33-35]. The Mg-4Li anode with lower values of the corrosion current density is stable. It can be well stored in the electrolyte. As the current density increases, it may not be activated quickly, exhibiting weak activity. The corrosion current density of Mg-4Li-3AlSi alloy is larger than that of Mg-4Li. But its corrosion current density is

still less than that of Mg-12Li and Mg-12Li-3AlSi alloy. In general, there may be no relationship between the corrosion current density and the corrosion potential [36]. Magnesium alloys with more negative corrosion potential can also have smaller corrosion current density, which has been supported by some literature research. [37, 38].

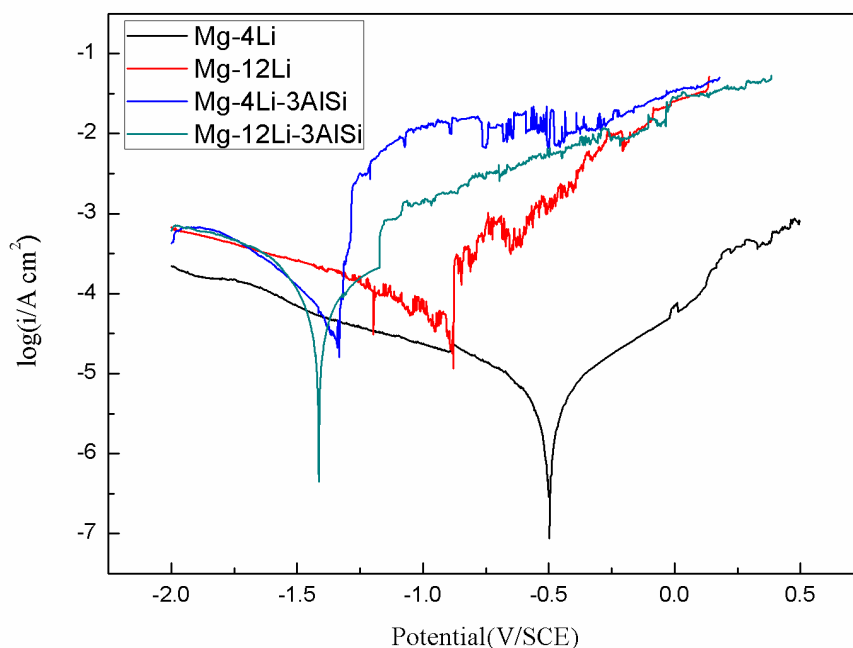


Figure 6. Polarization curves in 3.5 wt% NaCl solution of Mg-4Li, Mg-4Li-3AlSi, Mg-12Li.

Table 1. Corrosion potential (E_{corr}) and corrosion current density (i_{corr}) derived from different systems.

| | E_{corr} | i_{corr} |
|---------------|------------|-----------------------|
| Mg-4Li | -0.498 | 2.84×10^{-6} |
| Mg-4Li-3AlSi | -1.414 | 5.41×10^{-5} |
| Mg-12Li | -0.878 | 2.38×10^{-4} |
| Mg-12Li-3AlSi | -1.341 | 4.71×10^{-4} |

In order to further determine the characteristics of the corrosion resistances of different alloys. Electrochemical impedance spectroscopy (EIS) measurements on specimens under 3.5wt% NaCl solution are depicted in Fig 7. Different alloys all show a remarkable stability in 3.5wt% NaCl solution. All four alloys have only one capacitance loop across the frequency range. The alloy shows more active behavior. Its electrochemical process is activated without the action of the surface membrane. [32] The Bode plots which is related to the impedance modulus and the phase angle is given respectively. Compared with Mg-4Li-3AlSi and Mg-12Li-3AlSi alloys, Mg-4Li and Mg-12Li have greater impedance modulus, which means that the first two samples are more resistant to corrosion. This phenomenon is consistent with the corrosion current density listed in Table 2.

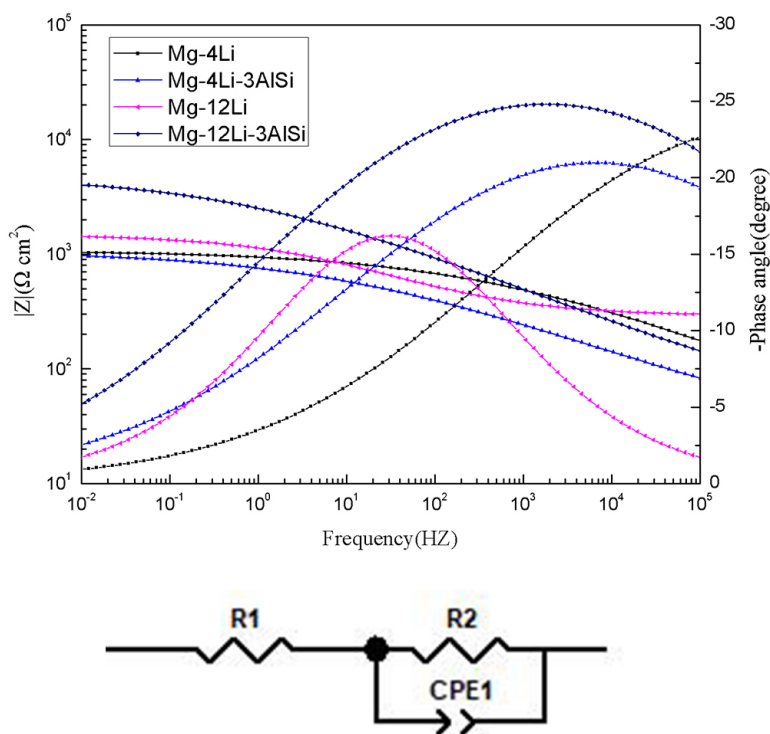


Figure 7. EIS plots obtained on Mg-4Li, Mg-4Li-3AlSi, Mg-12Li, Mg-12Li-3AlSi and Equivalent circuits used to fit EIS plots.

Fig. 7 shows the measured EIS fitted by Z-view software using the equivalent circuits depicted. In these circuits, R_s is a solution resistance. R_t are the charge transfer resistance and a $Mg(OH)_2$ film resistance, respectively. Because of the non-ideal capacitive behavior, the constant phase element is used. CPE-T and CPE-P instead of double capacitor and $Mg(OH)_2$ capacitor, respectively. The fitted results are listed in Table 2. It can be seen from the data of R_t that the Mg-12Li, Mg-4Li-3AlSi and Mg-12Li-3AlSi alloys are significantly lower than those of Mg-4Li, indicating that these three alloys are unstable. As proved by the corrosion current densities listed in Table 1. The Mg-4Li shows a larger R_t and has a weaker activity in the constant current discharge.

Table 2. Fitted parameters for EIS spectrum depicted in Figure 7.

| | R_s | $CEP-T$ | $CEP-P$ | R_t |
|---------------|-------|-------------------------|---------|-------|
| Mg-4Li | 36.26 | 11.473×10^{-5} | 0.326 | 4809 |
| Mg-4Li-3AlSi | 22.76 | 24.131×10^{-5} | 0.31 | 1034 |
| Mg-12Li | 28.83 | 17.78×10^{-5} | 0.448 | 1190 |
| Mg-12Li-3AlSi | 7.828 | 7.906×10^{-5} | 0.311 | 1058 |

4. CONCLUSIONS

1. The corrosion resistance of α -phase alloys (Mg-4Li and Mg-4Li-3AlSi) are much better than that of β -phase alloys (Mg-12Li and Mg-12Li-3AlSi).

2. Both Mg-4Li (α -phase) alloy and Mg-12Li (β -phase) alloy, the addition of Al-Si master alloy will cause the hydrogen evolution rate increase and the corrosion resistance decline. Hydrogen evolution rates on the same alloy surface are different. The loose fracture region is the main reason for the fast hydrogen evolution rate.

3. The surface phases of Mg-Li-AlSi alloys after hydrogen evolution are mainly α -Mg, β -Li, Mg(OH)₂, Al₂O₃ and Mg₂Si.

ACKNOWLEDGEMENTS

This work was supported by Chongqing Science Foundation of China (Nos. cstc2017jcyjBX00036, cstc2016jcyjA0426), the National Natural Science Foundation of China (No. 51778088), and the “Plan of Zhongxin” of Chongqing.

References

1. W. Xu, N. Birbilis, G. Sha, Y. Wang, J.E. Daniels, Y. Xiao and M. Ferry, *Nature Mater.*, 14 (2015) 1229.
2. J. Qiao, H. Jia, P K. Liaw, *Mater. Sci. Eng.*, R, 100 (2016) 1.
3. Z. Zhao, Z. Sun, W. Liang, Y. Wang, L. Bian., *Mater. Sci. Eng.*, A, 702 (2017) 206.
4. D. Wang, J. Zhang, J. Xu, Z. Zhao, W. Chen, C. Xu, *J. Magnesium Alloys*, 2 (2014) 78.
5. A.A. Luo, *Mater. Sci. Forum*, 419 (2003) 57.
6. M. Bamberger, G. Dehm, *Annu. Rev. Mater. Rev.*, 38 (2008) 505.
7. B.L. Mordike, T. Ebert, *Mater. Sci. Eng.*, A, 302 (2001) 37
8. H. Yu, C. Li, Y. Xin, A. Chapuis, X. Huang and Q. Liu, *Acta Mater.*, 128 (2017) 313.
9. B. Feng, Y. Xin, F. Guo, H. Yu, Y. Wu, and Q. Liu. *Acta Mater.*, 120(2016) 379.
10. N.L. Sukiman, H. Shi, R.K. Gupta, R.G. Buchheitc, and N. Birbilisa, *J. Electrochem. Soc.*, 160 (2013) 299.
11. D.K. Ivanou, M. Strykevich, A.D. Lisenkov, M.L. Zheludkevich, H.B. Xue, S.V. Lamaka, and M.G.S. Ferreira, *Corros. Sci.*, 73 (2013) 300.
12. S.A. Salman, R. Mori, R. Ichino, and M. Okido, *Mater. Trans.*, 51 (2010) 1109.
13. X.B. Chen, N. Birbilis, T.B. Abbott, *Corrosion*, 67 (2011) 035005.
14. G. Zhang, L. Wu, A. Tang, S. Zhang, B. Yuan, Z. Zheng, and F. Pan, *Adv. Mater. Interfaces*, 4 (2017) 1700163.
15. L. Wu, F. Pan, Y. Liu, G. Zhang and A. Atrens , *Surf. Eng.*, (2017) 1.
16. L. Wu, D. Yang, G. Zhang, Z. Zhang, S. Zhang, A. Tang, F. Pan, *App. Surf. Sci.*, 431 (2018) 177.
17. G. Zhang, L. Wu, A. Tang, B. Weng, A. Atrens, S. Ma, Lei Liu, and F. Pan, *RSC Adv.*, 8 (2018) 2248.
18. L. Wu, G. Zhang, A. Tang, Y. Liu, A. Atrens, and F. Pan, *Int. J. Electrochem. Sci.*, ,164 (2017) C339.
19. L. Wu, Z. Zheng, F. Pan, A. Tang, G. Zhang, and L. *Int. J. Electrochem. Sci.*, 12 (2017)6352-.
20. J. Liu, X. Lv, J. Li, et al., *J. Alloys Compd.*, 725 (2017) 1313.
21. Y. Xu, Y. Li, S. Sang, B. Ren, Q. Qin, and J. Yang , *Ceram. Inter.*, 40 (2014) 13169.
22. M. R. Loghman-Estarki, R. S. Razavi, H. Jamali, *Ceram. Inter.*, 42 (2016) 12825.

23. Y. Zeng, B. Jiang, R.H. Li, J.J. He, X.S. Xia, and F.S. Pan, *Mater. Sci. Eng., A*, 631 (2015) 189.
24. D.K. Xu, B.J. Wang, C.Q. Li, *Mater. Des.*, 69 (2015) 124.
25. X.Y. Guo, R.Z. Wu, L.J. Huang, *Mater. Sci. Eng., A*, 53 (2014) 528.
26. F.R. Cao, F. Xia, H.L. Hou, H. Ding, and Z.Q. Li, *Mater. Sci. Eng., A*, 637 (2015) 89.
27. A. A. Nayeb-Hashemi, J. B. Clark, A. D. Pelton, *J. Phase Equilib.*, 5 (1984) 365.
28. R. Wu, Y. Yan, G. Wang, L.E. Murr, W. Han, Z. Zhang, and M. Zhang, *Int. Mater. Rev.*, 60 (2015) 65.
29. Z.L. Zhao, X.G. Xing, Y. Luo, Y.D. Wang, and W. Liang, *J. Iron Steel Res.Int.*, 24 (2017) 426.
30. R. M. Poths, M. W. Rainforth, E. J. Palmiere, *Mater. Sci. Forum*, 426 (2003) 1255.
31. Y. Song, D. Shan, R. Chen, and E.H. Han, *Corros. Sci.*, 51 (2009) 1087.
32. R. Udhayan, D. P. Bhatt, *J. Power Sources*, 63 (1996) 103.
33. N. Wang, R. Wang, C. Peng, B. Peng, and Y. Feng, *Electrochim. Acta*, 149 (2014) 193.
34. N. Wang, R. Wang, C. Peng, and Y. Feng, *Corros. Sci.*, 81 (2014) 85.
35. N. Wang, R. Wang, C. Peng, Y. Feng, and B. Chen, *Corros. Sci.*, 64 (2012) 17.
36. M. Zhao, M. Liu, G. Song, and A. Atrens, *Corros. Sci.*, 50 (2008) 3168.
37. T. Cain, S.B. Madden, N. Birbilis, and J.R. Scully, *J. Electrochem. Soc.*, 162 (2015) 228.
38. G. Song, A. Atrens, M. Dargusch, *Corros. Sci.*, 41 (1999) 249.

© 2018 The Authors. Published by ESG (www.electrochemsci.org). This article is an open access article distributed under the terms and conditions of the Creative Commons Attribution license (<http://creativecommons.org/licenses/by/4.0/>).